UCSF

UC San Francisco Previously Published Works

Title

Novel SOX10 indel mutations drive schwannomas through impaired transactivation of myelination gene programs

Permalink

https://escholarship.org/uc/item/6zq333xt

Journal

Neuro-Oncology, 25(12)

ISSN

1522-8517

Authors

Williams, Erik A
Ravindranathan, Ajay
Gupta, Rohit
et al.

Publication Date

2023-12-08

DOI

10.1093/neuonc/noad121

Peer reviewed

Neuro-Oncology

Novel *SOX10* indel mutations drive schwannomas through impaired transactivation of myelination gene programs

Erik A. Williams[†1,©]**, Ajay Ravindranathan**[†]**, Rohit Gupta, Nicholas O. Stevers**[©]**, Abigail K. Suwala**[2]**, Chibo Hong, Somang Kim, Jimmy Bo Yuan, Jasper Wu, Jairo Barreto, Calixto-Hope G. Lucas, Emily Chan, Melike Pekmezci, Philip E. LeBoit, Thaddeus Mully, Arie Perry, Andrew Bollen, Jessica Van Ziffle, W. Patrick Devine, Alyssa T. Reddy, Nalin Gupta**[©]**, Kristen M. Basnet, Robert J.B. Macaulay, Patrick Malafronte, Han Lee, William H. Yong, Kevin Jon Williams, Tareq A. Juratli, Douglas A. Mata, Richard S.P. Huang, Matthew C. Hiemenz, Dean C. Pavlick, Garrett M. Frampton, Tyler Janovitz, Jeffrey S. Ross, Susan M. Chang, Mitchel S. Berger, Line Jacques**[©]**, Jun S. Song**[©]**, Joseph F. Costello**[©]**, and David A. Solomon**[©]

All author affiliations are listed at the end of the article

[†]Contributed equally.

Corresponding Author: David A. Solomon, University of California, San Francisco, 513 Parnassus Ave, Health Sciences West 451, San Francisco, CA 94143, USA (david.solomon@ucsf.edu).

[1]Present address: Department of Pathology and Laboratory Medicine, University of Miami, Sylvester Comprehensive Cancer Center, and Jackson Memorial Hospitals, Miami, Florida, USA.

[2]Present address: Department of Neuropathology, Institute of Pathology, Heidelberg University Hospital and Clinical Cooperation Unit Neuropathology, German Cancer Research Center (DKFZ), Heidelberg, Germany.

Abstract

Background. Schwannomas are common peripheral nerve sheath tumors that can cause severe morbidity given their stereotypic intracranial and paraspinal locations. Similar to many solid tumors, schwannomas and other nerve sheath tumors are primarily thought to arise due to aberrant hyperactivation of the RAS growth factor signaling pathway. Here, we sought to further define the molecular pathogenesis of schwannomas.

Methods. We performed comprehensive genomic profiling on a cohort of 96 human schwannomas, as well as DNA methylation profiling on a subset. Functional studies including RNA sequencing, chromatin immunoprecipitation-DNA sequencing, electrophoretic mobility shift assay, and luciferase reporter assays were performed in a fetal glial cell model following transduction with wildtype and tumor-derived mutant isoforms of *SOX10*.
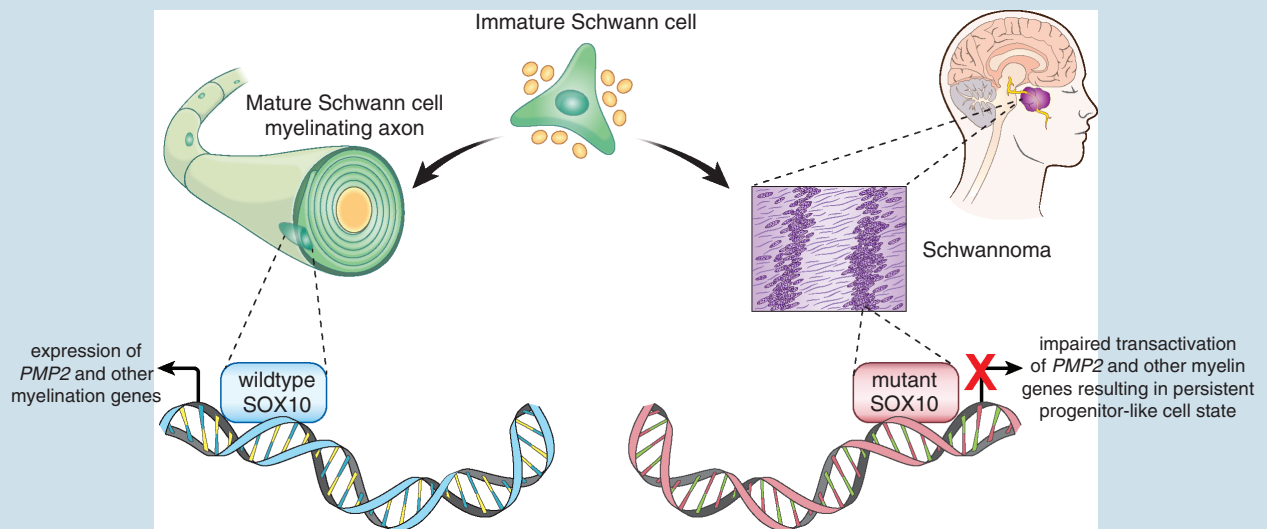
Results. We identified that nearly one-third of sporadic schwannomas lack alterations in known nerve sheath tumor genes and instead harbor novel recurrent in-frame insertion/deletion mutations in *SOX10*, which encodes a transcription factor responsible for controlling Schwann cell differentiation and myelination. *SOX10* indel mutations were highly enriched in schwannomas arising from nonvestibular cranial nerves (eg facial, trigeminal, vagus) and were absent from vestibular nerve schwannomas driven by *NF2* mutation. Functional studies revealed these *SOX10* indel mutations have retained DNA binding capacity but impaired transactivation of glial differentiation and myelination gene programs.

Conclusions. We thus speculate that *SOX10* indel mutations drive a unique subtype of schwannomas by impeding proper differentiation of immature Schwann cells.

Key Points

- Approximately 30% of sporadic schwannomas harbor somatic indel mutations in the *SOX10* gene.
- Schwannomas arising from nonvestibular cranial nerves are enriched for *SOX10* indel mutations.
- *SOX10* indel mutations impair transactivation of glial differentiation and myelination genes.

Graphical Abstract

Immature Schwann cell

Mature Schwann cell myelinating axon

Schwannoma

expression of *PMP2* and other myelination genes

wildtype SOX10

mutant SOX10

impaired transactivation of *PMP2* and other myelin genes resulting in persistent progenitor-like cell state

Importance of the Study

We have uncovered a new molecular mechanism responsible for nearly one-third of sporadic schwannomas—recurrent insertion/deletion mutations in *SOX10*. We demonstrate these *SOX10* indel mutations have retained DNA binding capacity but impaired transactivation of glial differentiation and myelination gene programs, and therefore likely cause schwannomas by blocking differentiation of immature Schwann cells.

Schwannomas are the most common nerve sheath tumor that develop from Schwann cells whose principal function is producing the myelin sheaths that insulate nerve fibers of the peripheral nervous system.[1] Schwannomas occur throughout the body, arising from cranial nerves, paraspinal nerve roots, and peripheral nerves in the soft tissue and skin. While typically slow-growing benign tumors, they can cause significant morbidity depending on location and adjacent structures that are compressed over time, particularly those involving cranial nerves such as hearing loss for schwannomas of the vestibular nerve. There is a peak incidence in the 4th to 6th decades of life, but they can arise throughout childhood or adulthood. Complete surgical resection can be curative but may

result in permanent nerve injury. Furthermore, complete resection is not always possible depending on tumor location that can result in local recurrence and progression over time, necessitating additional resection or radiation therapy for disease control and symptom management. Effective molecularly targeted therapy for schwannomas has not been developed to date.

A subset of schwannomas arises in the setting of heritable syndromes. Neurofibromatosis type 2 (NF2) is an autosomal dominant syndrome caused by heterozygous germline mutation in the *NF2* gene on chromosome 22q12.2, which encodes the Merlin protein. Patients with NF2 often develop bilateral vestibular schwannomas, as well as nonvestibular schwannomas,

multiple meningiomas, and spinal ependymomas.[2] Schwannomatosis is an autosomal dominant syndrome caused by heterozygous germline mutations in either the *SMARCB1* gene on chromosome 22q11.23 (which encodes the chromatin remodeling factor INI1/BAF47) or the *LZTR1* gene on chromosome 22q11.21 (which encodes a leucine zipper-like transcriptional regulator). Patients with *SMARCB1*- and *LZTR1*-associated schwannomatosis often develop multiple painful nonvestibular schwannomas in the absence of meningiomas or other tumor types.[3–6] Although studying patients with these heritable syndromes has provided insight into schwannoma pathogenesis, more than 90% of schwannomas are solitary and sporadic. Genetic analyses have revealed biallelic somatic *NF2* inactivation in approximately 50% of sporadic schwannomas,[7–13] while a recent study identified a novel *SH3PXD2A-HTRA1* in-frame gene fusion in a small subset (<10%) of sporadic schwannomas.[11] However, the molecular drivers responsible for a substantial subset of sporadic schwannomas remain unknown.

In this study, we performed targeted genomic profiling with ultra-deep sequencing depth (>500× mean coverage) coupled with careful bioinformatic assessment for insertion/deletion mutations to identify a new genetic driver of nearly one-third of sporadic schwannomas—in-frame insertion/deletion mutations in the *SOX10* gene, which encodes a homeobox transcription factor known to be critical for differentiation of Schwann cells.[14–16] Notably, these novel *SOX10* indel mutations in schwannomas were all somatic (tumor-acquired) and uniformly clustered at the carboxy terminal end of the high-mobility group (HMG)-box domain. This is in contrast to the mostly truncating loss-of-function germline mutations scattered throughout the *SOX10* gene (or occasionally whole gene deletion) that are known to cause Waardenburg syndrome type 4 (Online Mendelian Inheritance in Man # 613266), which is associated with a variable spectrum of sensorineural hearing loss, abnormal pigmentation of the hair and skin, aganglionic megacolon (Hirschsprung disease), peripheral demyelinating neuropathy, central dysmyelinating leukodystrophy, seizures/tremors, and early death.[17–19] Importantly, this syndrome does not include schwannoma, indicating a likely divergent mechanism of action of the somatic *SOX10* indel mutations in schwannomas versus the mostly truncating germline mutations in patients with Waardenburg syndrome type 4. We therefore evaluated the functional mechanism by which these *SOX10* indel mutations fuel schwannoma development and uncovered a new paradigm in oncogenesis—recurrent mutations in a transcription factor responsible for controlling cell fate that promote tumorigenesis through impaired transactivation of tissue-specific differentiation gene programs.

Methods

Study Population and Tumor Specimens

The discovery cohort consisted of 39 pathologically confirmed schwannomas resected from 36 unique patients at a tertiary academic medical center (University of California San Francisco [UCSF]). The tumors were located at various anatomic sites and a subset had occurred in the setting of known genetic syndromes predisposing to schwannomas, which included two anatomically separate tumors each from three patients. The validation cohort consisted of 57 pathologically confirmed schwannomas resected from various anatomic sites of 57 unique patients that were sent for comprehensive genomic profiling (FoundationOneCDx) as part of clinical management at medical institutions across North America. The discovery cohort portion of this study was approved by the UCSF Committee on Human Research with a waiver of patient consent. As part of routine clinical practice at UCSF, all patients included in the discovery cohort signed an informed consent waiver to contribute de-identified data to scientific research projects. Approval for the validation cohort portion of the study, including a waiver of informed consent and a Health Insurance Portability and Accountability Act waiver of authorization, was obtained from the Western Institutional Review Board (Protocol No. 20152817). See Supplementary Methods for further details.

Histology and Immunohistochemistry

Detailed pathologic examination was performed retrospectively to investigate histologic and immunohistochemical features. See Supplementary Methods for further details including primary antibodies used.

Targeted Next-generation DNA Sequencing and Mutational Analysis for Discovery Cohort

Genomic DNA was extracted from formalin-fixed, paraffin-embedded tumor tissue from the 44 schwannian tumors of the discovery cohort using the QIAamp DNA FFPE Tissue Kit (Qiagen). Genomic DNA was also extracted from a peripheral blood sample from 15 patients using the QIAamp DNA Blood Midi Kit (Qiagen). Targeted next-generation sequencing was performed using the UCSF500 NGS Panel as previously described (gene list in Supplementary Table S23).[20–22] See Supplementary Methods for further details.

Targeted Next-generation DNA Sequencing and Mutational Analysis for Validation Cohort

Comprehensive genomic profiling for the validation cohort of 72 unique patient schwannian tumor samples was performed in a Clinical Laboratory Improvement Amendments-certified, College of American Pathologists-accredited laboratory (Foundation Medicine, Cambridge, MA) as previously described (gene list in Supplementary Table S24).[23] See Supplementary Methods for further details.

DNA Methylation Profiling of Schwannoma Tumor Samples

Genomic DNA from a subset of the schwannomas (*n* = 22) was bisulfite converted using the EZ DNA Methylation kit following the manufacturer's recommended protocol (Zymo Research). Bisulfite converted DNA was

then amplified, fragmented, and hybridized to Infinium EPIC 850k Human DNA Methylation BeadChips following the manufacturer's recommended protocol (Illumina). Methylation data were preprocessed using the minfi package (v.1.38.0) in R Bioconductor (v.3.5.3).[24] Functional normalization with NOOB background correction and dye-bias normalization was performed with the preprocessFunnorm function.[25,26] See Supplementary Methods for further details.

tSNE Dimensionality Reduction of DNA Methylation Data from Schwannoma Tumor Samples

The DNA methylation profiles of the 22 schwannomas were assessed together with 225 reference tumors spanning 10 nerve sheath tumor, CNS tumor, and sarcoma entities,[27,28] which were selected based on tumor types with a similar spinal/paraspinal or soft tissue locations and tumor types that might enter into the differential diagnosis based on overlapping morphologic appearance (sample manifest in Supplementary Table S9). Dimensionality reduction using t-distributed stochastic neighbor embedding (tSNE) was performed by Rtsne (v.0.16). See Supplementary Methods for further details.

Unsupervised Hierarchical Clustering of DNA Methylation Data from Nerve Sheath Tumor Samples

Unsupervised hierarchical clustering was performed with the hclust function in Rstats (v.3.6.0) to assess variation in DNA methylation patterns and determine any relevant epigenetic subgrouping among the 22 schwannoma tumor samples and 9 neurofibromas (NFB), 26 malignant peripheral nerve sheath tumors (MPNST), and 7 malignant melanotic nerve sheath tumors (MEL, SCHW) (sample manifest in Supplementary Table S10). The lmFit function from the Limma package (v.3.48.3) was used, with visualization performed using the R package ComplexHeatmap (v.2.0.0).[29] See Supplementary Methods for further details.

Differential DNA Methylation Analysis of Schwannoma Molecular Subtypes

The dmpFinder function from the minfi package (v.1.38.0) was applied on the β-value matrix to identify differentially methylated CpG sites among 17 schwannomas comprised of 8 with *SOX10* indel mutations and 9 with inactivating *NF2* mutations. From this differentially methylated probe (DMP) analysis, we identified the 1,050 CpG sites with adjusted P value < 0.05 and > 0.1 difference in mean β-value between the two molecularly defined subgroups. CpG annotation was performed using IlluminaHumanMethylationEPICanno.ilm10b4.hg19' (v.0.6.0). Unsupervised hierarchical clustering of these 17 schwannomas was performed using the derived 1,050 CpG site signature matrix with the hclust function in Rstats and visualized using ComplexHeatmap. The volcano plot function of methylR (v.1.0.1) was used to visualize the 100,000 CpG sites from

the DMP analysis with the lowest adjusted P-values. Visualization of methylation status at individual CpG sites mapped to the human genome was performed with the DMR.plot function in DMRcate (v.2.6.0).[30]

SOX10 cDNA Expression Vector Construction and Site-directed Mutagenesis

A human wildtype *SOX10* cDNA (CCDS11664, RefSeq NM_006941.4) with 3xFLAG sequence inserted at the 3′ end immediately preceding the TAA stop codon with flanking 5′ BamH1 and 3′ EcoR1 restriction sites was synthesized by GenScript and cloned into the pCDF1-MCS2-EF1-Puro lentiviral expression vector (System Biosciences). Two insertion mutations recurrently observed in human schwannoma samples were engineered into the pCDF1-SOX10-3xFLAG construct by site-directed mutagenesis using the QuikChange II XL kit (Stratagene) as directed by the manufacturer:

c.519_520insAAGTAC, p.Y173_Q174insKY (also annotated as c.514_519dup, p.K172_Y173dup)

c.529_530insCCCAGCCCAGGC, p.R176_R177insPQPR

See Supplementary Methods for further details.

Lentiviral Production and Infection

Empty pCDF1 vector or pCDF1-SOX10-3xFLAG wildtype and mutant expression vectors were co-transfected into HEK-293T cells with pVSV-G and pFIV-34N helper plasmids (System Biosciences) using FuGENE 6 (Roche) following the manufacturer's recommended protocol. Virus-containing conditioned medium was harvested 48 hours after transfection, filtered, and used to infect recipient SVG cells in the presence of 10 µg/mL polybrene.

Immortalized Human Fetal Glial Cell Cultures

SVG-p12 fetal glial cells derived from brain material dissected from 8 to 12-week old human embryos were obtained directly from ATCC (CRL-8621). See Supplementary Methods for further details.

Primary Human Schwannoma Cell Culture

Schwannoma tumor tissue surgically resected from the right ulnar nerve of an adult male was dissociated by mincing and enzymatic digestion using Liberase TM (Sigma cat # 5401119001) for 45 min at 37°C. Cells were grown on laminin coated plates (Sigma cat # L2020) in DMEM supplemented with 10% fetal bovine serum at 37°C in 5% CO_2. Genomic DNA was extracted, and targeted genomic profiling demonstrated a somatic *NF2* p.R466* nonsense mutation (RefSeq transcript NM_000268; chr22:g. 30,070,880C >T).

Western Blot

Total protein was extracted from stably transduced SVG cells, along with a primary human schwannoma cell

culture, U87MG glioblastoma cells (ATCC, cat# HTB-14), and SK-MEL-28 melanoma cells (ATCC, cat# HTB-72) in RIPA buffer supplemented with protease and phosphatase inhibitors (Pierce cat# PIA32959), resolved by SDS-PAGE, and immunoblotted following standard biochemical techniques. Primary antibodies used were SOX10 (Santa Cruz Biotechnology, cat# sc-365692, 1:500 dilution), SOX10 (Cell Signaling, cat #89356, clone D5V9L, 1:1,000 dilution), FLAG (Sigma-Aldrich, cat# F1804, clone M2, 1:1,000 dilution), phospho-ERK1/2 Thr202/Tyr204 (Cell Signaling, cat# 4370, clone D13.14.4E, 1:500 dilution), and alpha-tubulin (Abcam, cat# 18251, 1:10,000 dilution).

RNA-Seq Analysis of SVG Cells Transduced with Wildtype and Mutant *SOX10* Isoforms

Total RNA was extracted from SVG cells stably transduced with empty vector, *SOX10* wildtype, or *SOX10* mutant isoforms using TRIzol (Invitrogen). RNA sequencing libraries were prepared from oligo-d(T) selected RNA using the KAPA Stranded RNA-seq Library Prep Kit following the manufacturer's protocols. Paired-end (150 bp) sequencing was performed in a NovaSeq S4 flowcell on the NovaSeq 6000 platform (Illumina) at the QB3-Berkeley Genomics center at the University of California, Berkeley. Three separate library preparations and sequencing runs were performed for each sample. Trimmed sequence reads were mapped to GRCh38 using HISAT2 version 2.2.1 using default parameters.[31] Transcript count extraction was performed using the featureCounts function in the subRead package version 2.0.3. Differential gene expression analysis was performed using DESeq2 v3.10.[32] Volcano plots of significantly differentially expressed genes were generated using EnhancedVolcano package v1.10.0.[33] Differentially expressed transcripts with p-values of $< 1 \times 10^{-5}$ and log2 fold change > 1.2 were identified and prioritized as potentially biologically relevant genes. See Supplementary Methods for further details.

Quantitative RT-PCR Analysis

Total RNA was extracted from SVG cells stably transduced with empty pCDF1 vector, *SOX10* wildtype, or *SOX10* mutant isoforms using TRIzol (Invitrogen). RNA was reverse-transcribed and PCR-amplified using the StepOnePlus system (Applied Biosystems) with the Luna Universal One-Step RT-qPCR Kit (New England Biolabs, cat #E3005). See Supplementary Methods for further details including primers.

ChIP-seq Analysis of SVG Cells Transduced with Wildtype and Mutant *SOX10* Isoforms

Chromatin immunoprecipitation coupled with DNA sequencing (ChIP-seq) was performed on SVG cells stably transduced with FLAG-tagged *SOX10* wildtype or two tumor-derived *SOX10* mutant isoforms using the SimpleChIP Plus Sonication Chromatin IP Kit (Cell Signaling cat # 56383) with the mouse anti-FLAG clone M2 antibody (Sigma cat # F1804) following the manufacturer's instructions. See Supplementary Methods

for further details. Two independent ChIP reactions and DNA sequencing replicates were performed for each experimental sample.

Determination of Genome-wide SOX10 Binding Sites

Paired-end ChIP-seq reads were mapped to the human genome (GRCh38) using bowtie2 (version 2.4.2).[34] Mapped reads were filtered using the view command in samtools (version 1.12) with the options -h -F 4 -q 10.[35] Reads mapped to the same genomic coordinates were deduplicated using the markdup command in samtools with the option -r. Normalized signal tracks representing the genome-wide fragment density of samples were obtained by using the bamCoverage function in deepTools (version 3.2.1) with the options --normalizeUsing RPGC --extendReads --binSize 10 and bigwigCompare function with the options --operation ratio --binSize 10.[36] Peak calling for deduplicated reads derived from individual samples was performed using the callpeak command in MACS2 (version 2.2.5) with the options --format BAMPE --min-length 150 -g hs -q 0.3.[37] Peak locations were pooled across the two independent replicates to determine a consensus set of peaks using IDR (version 2.0.4) with the commands --input-file-type narrowPeak --rank q.value.[38] Genomic locations of consensus peaks were determined by keeping only intersecting peaks with irreproducible discovery rate < 0.1.

Gene Ontology Analysis of SOX10 Chromatin Binding Sites

The GREAT (version 4.0.4) web tool was used to perform gene ontology (GO) analysis of gene sets enriched near SOX10 binding sites.[39] All genomic peak locations derived from IDR were used as inputs to GREAT. For every gene, regulatory regions were constructed by first defining a proximal regulatory region consisting of genomic locations 5 kilobases (kb) upstream and 1 kb downstream of the transcription start site (TSS). Distal regulatory regions were defined by extending the proximal regulatory region by 500 kb or until the proximal regulatory region meets the edge of the proximal regulatory region of the nearest gene, whichever is shorter. Full regulatory regions were defined to consist of the union of proximal and distal regulatory regions. Genes were considered bound by SOX10 if the SOX10 binding site was located within the full regulatory region. Gene set annotations were selected from the Gene Ontology Biological Process database.[40] Functional gene sets enriched in SOX10 binding sites were determined using Fisher's exact test with $q < 0.05$.

DNA Motif Analysis of SOX10 Binding Sites

Motif analysis was performed using the default parameters of the STREME web tool from the MEME suite (version 5.5.1).[41,42] Input sequences to STREME were derived from the sequences in a 201 bp region centered at the peak summits in the *SOX10* wildtype samples as determined by IDR, where nucleotides in known genomic repeat regions were masked. Sequence motifs were determined by computing

the Kullback-Leibler (KL) divergence of the resulting position-specific scoring matrix (PSSM) with the uniform distribution.

PMP2 Promoter Reporter Assay

Luciferase reporter assays were performed in SVG cells stably transduced with empty vector, *SOX10* wildtype, or *SOX10* mutant isoforms using a luciferase reporter construct in the pGL2 vector backbone containing a segment of the promoter region of the *PMP2* gene as previously described that includes a known SOX10 binding site.[43] Luciferase activity was measured using the Dual Luciferase Reporter Assay System (Promega cat# E1910). See Supplementary Methods for further details.

PMP2 Promoter Electrophoretic Mobility Shift Assay

Nuclear extracts were prepared from SVG cells stably transduced with empty vector, *SOX10* wildtype, or *SOX10* mutant isoforms using the Nuclear Extract kit (Active Motif cat# 40010) according to the manufacturer's protocol. A 26 base pair oligonucleotide segment of the human *PMP2* promoter containing a confirmed SOX10 binding site[43] was synthesized with and without a 5′ biotin end-label (Integrated DNA Technologies). This double-stranded oligonucleotide segment of the human *PMP2* promoter was used to perform electrophoretic mobility shift assays (EMSA) using the Gelshift Chemiluminescent EMSA kit (Active Motif cat# 37341) according to the manufacturer's instructions. See Supplementary Methods for further details including oligonucleotide probe sequence.

Statistics

Student's *t*- and χ^2 tests were used to compare variables between patient cohorts. Kaplan–Meier plots were used to estimate disease-specific and progression-free survival. Disease-specific survival was defined as the time from initial diagnostic surgical procedure until death due to disease. Progression-free survival was defined as the time from initial diagnostic surgical procedure until local recurrence for gross totally resected tumors or progressive tumor growth for subtotally resected tumors. Censoring was performed at either the last clinical follow-up visit or death due to unrelated cause. All statistical analyses were performed using GraphPad Prism version 7.04. All experiments were performed with independent biological replicates, and statistics were derived from biological replicates as indicated in each figure legend. Bar plots show means, and error bars represent standard deviation of the means.

Results

Novel *SOX10* Indel Mutations in Sporadic Schwannomas

To advance understanding of schwannoma pathogenesis, we performed genomic profiling on a discovery cohort of 39 pathologically confirmed schwannomas resected from 36 patients (Figure 1A, Supplementary Tables S1–S4). Biallelic *NF2* inactivation was identified in 24 tumors (62%), of which a subset had accompanying mutations in *LZTR1* or *SMARCB1*. *SH3PXD2A-HTRA1* fusion was identified in 5 tumors (13%). The remaining 10 schwannomas lacked alterations in known nerve sheath tumor genes. Eight of these schwannomas (21% of the discovery cohort) were discovered to harbor previously unrecognized in-frame insertion or deletion (indel) mutations within the *SOX10* gene. There were six tumors with insertions ranging in length from 3 to 15 bp, and two tumors with the identical 69 base pair deletion. These novel indel mutations were uniformly located in the region encoding the C-terminal end of the HMG-box domain (Figure 1B), which is the DNA binding motif of the SOX10 protein and is a region that is highly conserved from humans through lower vertebrates (Figure 1C). The *SOX10* indel mutations were confirmed to be somatic in origin in five of the patients for whom sequencing of a normal constitutional DNA sample was performed. In the other three *SOX10*-mutant tumors, the variant allele frequency was consistent with being somatically acquired as well. To confirm these findings, we performed genomic profiling on a separate validation cohort of 57 pathologically confirmed schwannomas (Supplementary Figure S1, Supplementary Tables S5-S6). Similar *SOX10* indel mutations were found in 14 tumors (25%) that were also present at variant allele frequencies consistent with somatically acquired origin.

Combining the discovery and validation cohorts, we identified a total of 22 unique patients with *SOX10*-mutant schwannomas. None of these 22 patients had clinical evidence of NF2 or schwannomatosis, with an overall frequency of *SOX10* mutation in sporadic/non-syndromic schwannomas of 29% (22/77). The 22 *SOX10*-mutant tumors lacked alterations in known genetic drivers of schwannomas (*NF2*, *HTRA1*, *LZTR1*, *SMARCB1*), neurofibromas (*NF1*), or malignant peripheral nerve sheath tumors (*NF1*, *CDKN2A*, *SUZ12*, *EED*, *TP53*).[44] Moreover, we found that these novel *SOX10* indel mutations were absent from other schwannian lineage nerve sheath tumors, including *ERBB2*-mutant hybrid schwannoma-neurofibromas (*n* = 8) and *PRKAR1A*-mutant malignant melanotic nerve sheath tumors (formerly termed melanotic schwannoma, *n* = 12) (Figure 1A, Supplementary Figure S1).[45,46] A large majority of *NF2*-mutant schwannomas (96% in the discovery cohort, 78% in the validation cohort) had either monosomy or copy-neutral loss of heterozygosity (LOH) of chromosome 22q that functions as the mechanism for eliminating the wildtype *NF2* allele (Supplementary Table S4, Supplementary Figure S1). In contrast, although the *SOX10* locus is also on chromosome 22q, monosomy or LOH of chromosome 22q was present in only 9 of the 22 *SOX10*-mutant schwannomas (41%).

Histopathologic analysis of *SOX10*-mutant schwannomas revealed conventional morphologic features of schwannoma including spindled tumor cells and nuclear palisades termed Verocay bodies (Figure 1D, Supplementary Figure S2, Supplementary Table S7). As with normal Schwann cells and schwannomas with other molecular drivers, *SOX10*-mutant schwannoma tumor cells were found to robustly express nuclear SOX10 protein by immunohistochemistry, indicating the indel mutations do not cause protein degradation or abnormal intracellular trafficking/localization (Figure 1D, Supplementary

Figure 1. **Recurrent *SOX10* indel mutations in sporadic schwannomas lacking alterations in known nerve sheath tumor genes.** (A) Genomic profiling on a discovery cohort of 39 schwannomas identified recurrent somatic mutations of the *SOX10* gene in 8/30 (27%) sporadic/nonsyndromic schwannomas that lacked alterations in all other known nerve sheath tumor genes. See Supplementary Figure S1 for results of genomic profiling on an independent validation cohort of 57 additional schwannomas. (B) Diagram of the recurrent in-frame insertion and deletion mutations identified in *SOX10*, which all cluster at the C-terminus of the HMG-box DNA-binding domain of the encoded homeobox transcription factor. The two bolded mutations (p.Y173_Q174insKY [also annotated p.K172_Y173dup] and p.R176_R177insPQPR) were those used in functional studies. (C) Amino acid sequence of SOX10 in the region of the carboxy terminal end of the HMG domain (green shading) where the recurrent indel mutations in schwannomas are located demonstrating a high degree of conservation from humans through lower vertebrates including mouse and zebrafish. Uniprot ID for amino acid sequence: *Homo sapiens*, P56693-1; *Pan troglodytes*, A0A2J8LNY1; *Loxodonta africana*, G3U829; *Mus musculus*, Q04888; *Rattus norvegicus*, O55170; *Gallus gallus*, Q9W757; *Danio rerio*, Q90XD1. (D) Histopathology of the *SOX10*-mutant schwannoma arising from the right trigeminal nerve (cranial nerve V) in a 12-year-old male patient. Scale bar, 50 μm. (E) Unsupervised hierarchical clustering of genome-wide DNA methylation data for 22 schwannomas of varying genotypes along with 42 reference nerve sheath tumors. K-means clustering segregated these tumors into 4 epigenetic groups, which recapitulated the associated histopathologic diagnoses. Shown is a heatmap of the 20,000 most differentially methylated probes amongst the 64 tumors. See Supplementary Table S10 for sample manifest.
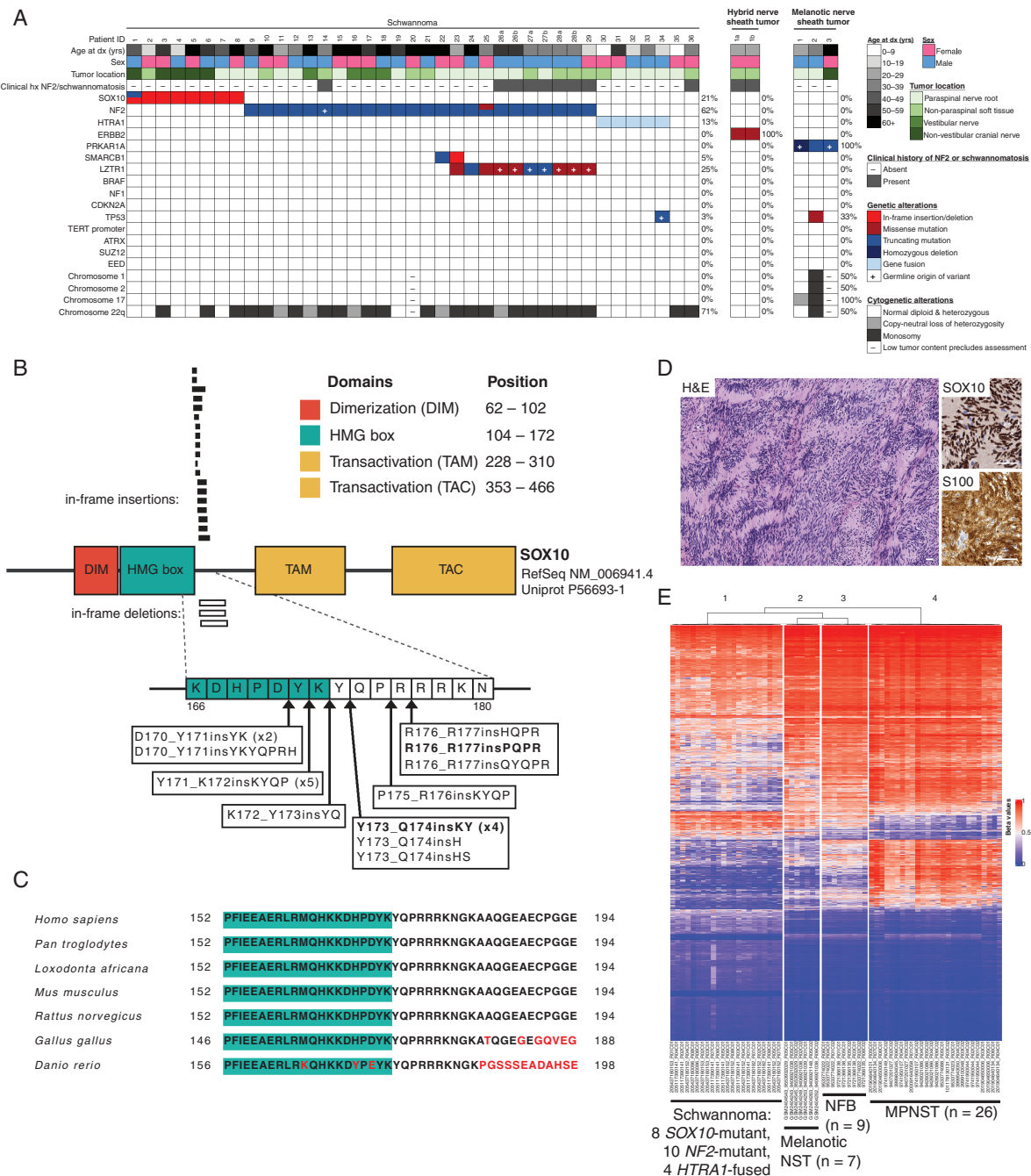
Figure S3, Supplementary Table S8). Genome-wide DNA methylation interrogation of *SOX10*-mutant, *NF2*-mutant, and *SH3PXD2A-HTRA1*-fused schwannomas revealed an overall similar epigenetic profile (Figure 1E, Supplementary Figure S4, Supplementary Tables S9-S10), thereby providing further support that *SOX10*-mutant tumors are a molecular subtype of schwannoma and not an altogether divergent nerve sheath tumor entity.

Fine Epigenetic Mapping Reveals Schwannomas with *SOX10* Indel Mutation have a Distinct Signature Compared to Those with *NF2* Mutation

We derived a signature matrix of 1,050 differentially methylated CpG sites that reliably segregated a cohort of 17 schwannomas into those with *SOX10* indel mutation versus those with *NF2* mutation (Figure 2A, Supplementary Table S11). Several of the most differentially methylated CpG sites between the two molecular subgroups were clustered together at the 5′ end of the *MEIS1* gene (Figure 2B-C), which encodes a member of the three amino acid loop extension (TALE) homeodomain transcription factor family that is critical for neural crest development including cranial nerves.[47] These CpG sites in the 5′ end of *MEIS1* were significantly hypomethylated in *SOX10*-mutant schwannomas compared to *NF2*-mutant tumors, indicating that DNA methylation status of the *MEIS1* gene may be a hallmark for distinguishing schwannomas arising due to different genetic alterations and its differential methylation might potentially be critical to their underlying pathogenesis.

Schwannomas Arising from Nonvestibular Cranial Nerves are Enriched for *SOX10* Indel Mutations

Among the 22 patients with *SOX10*-mutant schwannomas, there was a near-equal sex distribution (10 males, 12 females). Median age at initial schwannoma diagnosis was 52 years (range 12–75 years), which included multiple adolescents (Figure 3A). Many *SOX10*-mutant schwannomas involved nonvestibular cranial nerves including the facial, trigeminal, vagus, and spinal accessory nerves, but also the paraspinal nerve roots or more distally along nerves in the extremities (eg median nerve, brachial plexus) (Figure 3B-C). Among the 96 total genotyped schwannomas, 8 involved nonvestibular cranial nerves that included 7 with *SOX10* mutation (88%) and only 1 with *NF2* mutation (12%). Additionally, 25 of the 96 involved the vestibular nerve that included none with *SOX10* mutation (0%) and 23 with *NF2* mutation (95%). Thus, there was an enrichment for *SOX10* mutation in nonvestibular cranial nerve schwannomas versus *NF2* mutation in vestibular schwannomas ($P < 0.0001$ by Chi-square test). While no patients with *SOX10*-mutant schwannomas developed metastasis or died of disease during the available period of clinical follow-up, many of these patients had tumors that were challenging to completely surgically remove (particularly those involving the facial, trigeminal, or vagus nerves). Several patients with *SOX10*-mutant schwannomas experienced local recurrence after gross-total resection or tumor progression after subtotal resection which necessitated

additional treatment including radiotherapy (Figure 3D, Supplementary Tables S1 and S5). Thus, there is a clinical need to better understand the biology of and develop effective treatments for *SOX10*-mutant schwannomas.

Wildtype *SOX10* Controls Expression of Glial Differentiation and Myelination Gene Programs

Given the presence of recurrent in-frame variants that uniformly cluster at the C-terminal end of the HMG-box DNA-binding domain, we hypothesized that these novel *SOX10* indel mutations might drive schwannoma formation through either perturbing chromatin binding or impairing transcriptional activity after chromatin binding. To investigate this, we stably transduced SVG-p12 human fetal glial cells with either empty vector, a full-length wildtype human *SOX10* cDNA, or two different tumor-derived insertion mutant isoforms of *SOX10*. We utilized SVG-p12 cells as they are nonterminally differentiated glial cells from a fetal source that only express a minimal amount of endogenous SOX10 protein, thereby enabling our study of exogenous wildtype and mutant SOX10 isoforms to control gene expression programs responsible for glial differentiation and myelination in the context of immature glial cells. We observed a similar abundance of SOX10 protein following stable lentiviral transduction of SVG cells compared to the endogenous SOX10 protein levels present in a primary human schwannoma cell culture (Figure 4A), indicating that these stably transduced SVG cells represent an appropriate model system in which to investigate the effects of physiologic levels of exogenously expressed wildtype and mutant SOX10 isoforms.

Whole transcriptome RNA-sequencing with differential gene expression analysis of this SVG cell model revealed that wildtype *SOX10* induced a group of genes characteristic of mature myelinating glial cells, including *PMP2* (peripheral myelin protein 2), *PLP1* (proteolipid protein 1), *S100A1* (S100 calcium-binding protein A1), and *L1CAM* (L1 neuronal cell adhesion molecule) (Figure 4B-D, Supplementary Tables S12-S13). Gene Ontology analysis revealed enrichment of biologic processes including myelin biosynthesis and glial cell differentiation (Figure 4B, Supplementary Table S14).

SOX10 Indel Mutations Impair Transactivation of Myelination Gene Programs

Despite being expressed at equal or slightly higher levels than the wildtype protein, both *SOX10* indel mutants failed to activate expression of the myelination and glial differentiation gene programs induced by wildtype *SOX10*, including the *PMP2*, *PLP1*, and *L1CAM* genes (Figure 4C and E-F, Supplementary Figure S5, Supplementary Tables S15-S20). In contrast to other genetic alterations that drive nerve sheath tumors through hyperactivation of the RAS growth factor signaling pathway (eg *NF1*, *NF2*, and *LZTR1* mutations, *SH3PXD2A-HTRA1* fusion),[11,44,48,49] expression of *SOX10* mutant isoforms did not lead to increased ERK1/2 phosphorylation in SVG fetal glial cells (Figure 4G).

To study chromatin binding of the wildtype and mutant *SOX10* isoforms, we performed genome-wide ChIP-seq on
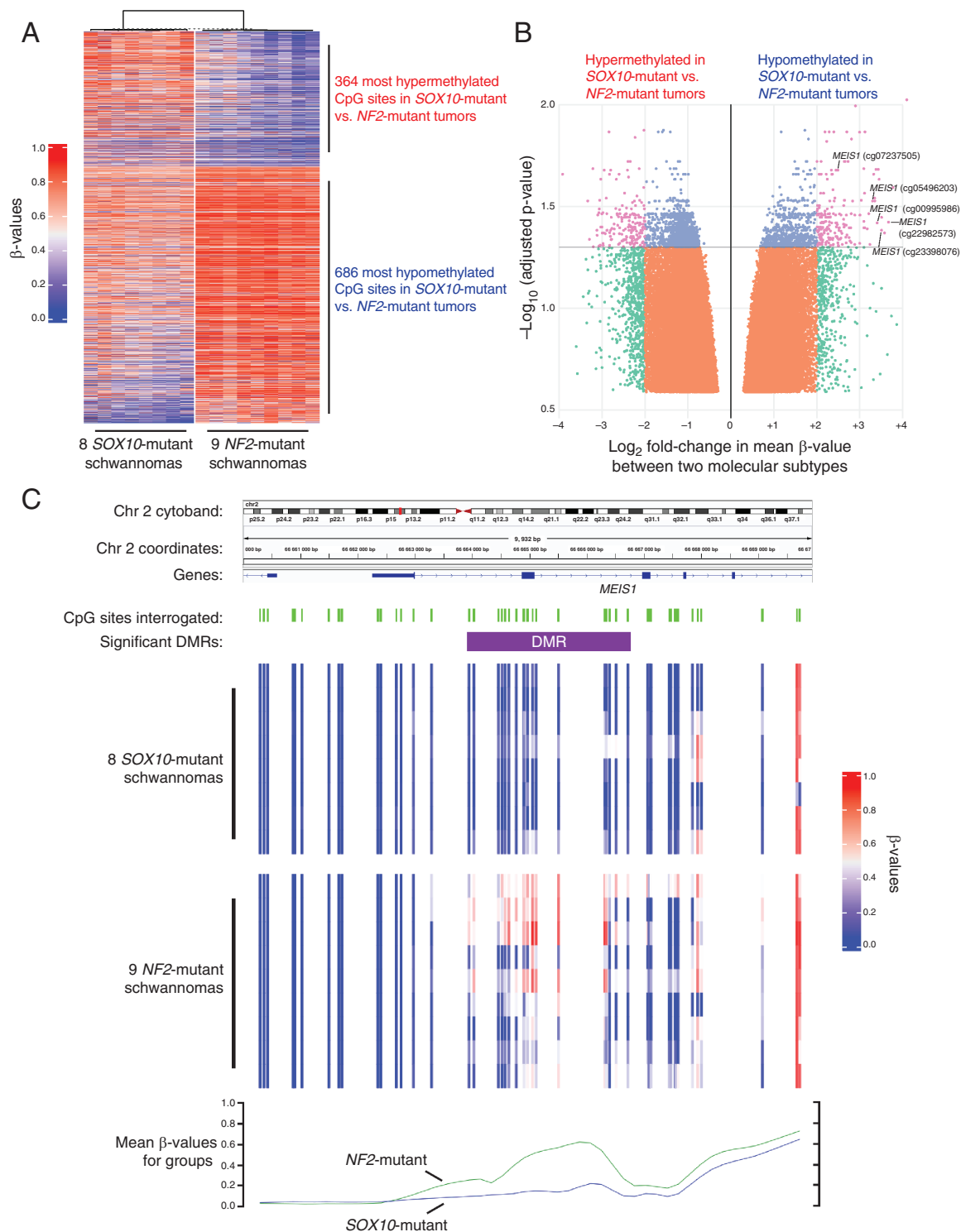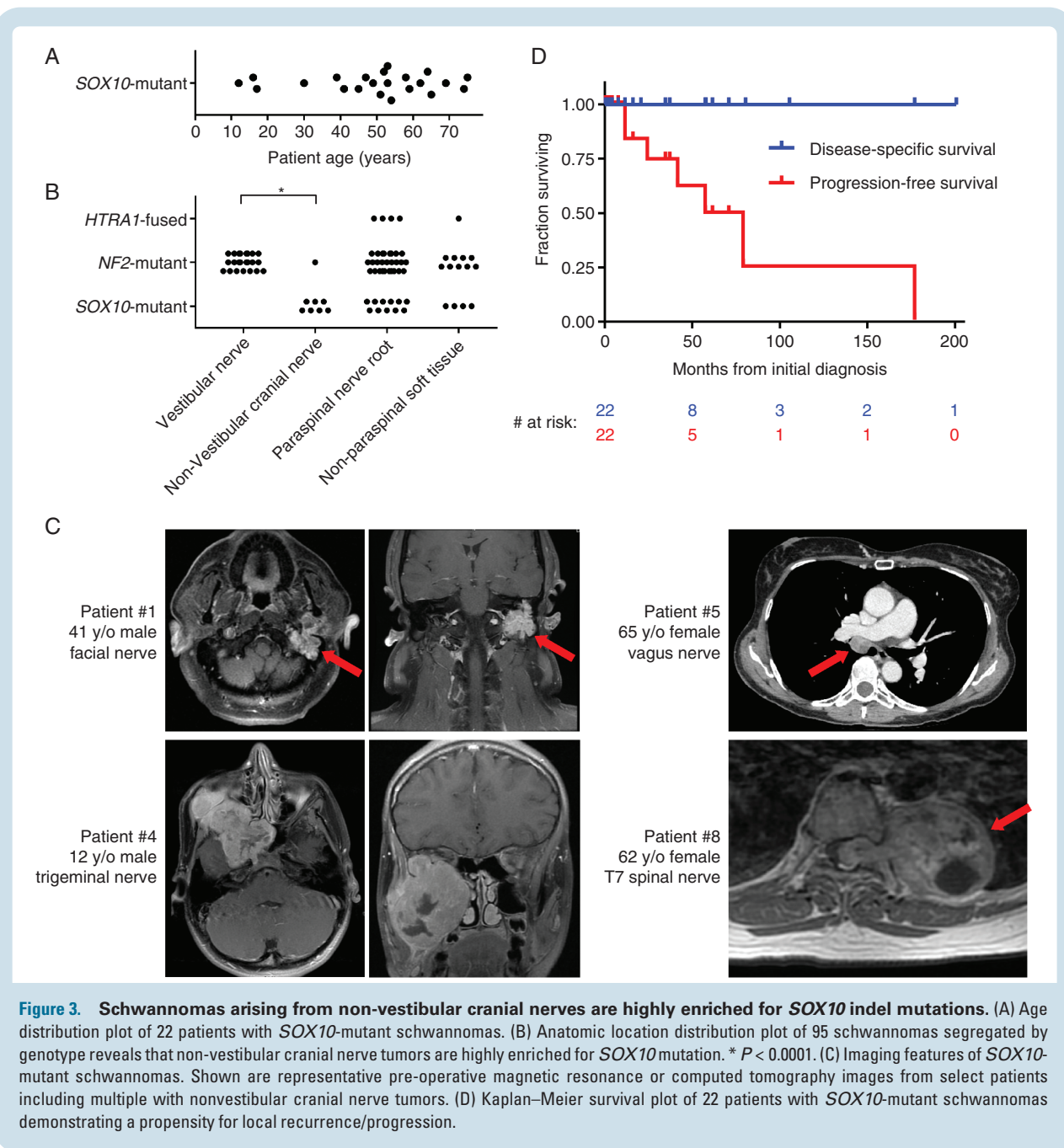
Figure 2.   **Schwannomas with *SOX10* indel mutation have a distinct epigenetic signature compared to those with *NF2* mutation.** (A) Unsupervised hierarchical clustering of DNA methylation data for 8 schwannomas with *SOX10* indel mutations and 9 schwannomas with inactivating *NF2* mutations. K-means clustering segregated these tumors into 2 epigenetic groups, which comprised those with *SOX10* indel mutation and those with *NF2* mutation. Shown is a heatmap of the 1,050 most differentially methylated probes amongst the 17 tumors. See Supplementary Table S11 for detailed annotations of these 1,050 differentially methylated CpG sites. **B,** Volcano plot of DNA methylation data for 8 schwannomas with *SOX10* indel mutations and 9 schwannomas with inactivating *NF2* mutations. The 100,000 CpG sites with the lowest adjusted p-values by DMP analysis are shown, and those CpG sites having adjusted p-values < 0.05 and greater than ± 2 log2 fold-change in mean β-values between the two molecular subgroups are colored pink. (C) Visualization of DNA methylation status at CpG sites within and immediately upstream of the *MEIS1* gene locus on chromosome 2p14 in 8 schwannomas with *SOX10* indel mutations and 9 schwannomas with inactivating *NF2* mutations.

Figure 3. **Schwannomas arising from non-vestibular cranial nerves are highly enriched for *SOX10* indel mutations.** (A) Age distribution plot of 22 patients with *SOX10*-mutant schwannomas. (B) Anatomic location distribution plot of 95 schwannomas segregated by genotype reveals that non-vestibular cranial nerve tumors are highly enriched for *SOX10* mutation. * $P < 0.0001$. (C) Imaging features of *SOX10*-mutant schwannomas. Shown are representative pre-operative magnetic resonance or computed tomography images from select patients including multiple with nonvestibular cranial nerve tumors. (D) Kaplan–Meier survival plot of 22 patients with *SOX10*-mutant schwannomas demonstrating a propensity for local recurrence/progression.

the SVG cells. We identified 1,777 high-confidence chromatin binding peaks in cells transduced with wildtype *SOX10*, which contained the known SOX10 DNA sequence binding motif ACAAAG (Figure 5A).[50] Gene Ontology biologic processes enriched in genes with chromatin binding peaks in the SOX10 wildtype samples included myelin assembly, neuron recognition, and regulation of neuronal synaptic plasticity (Figure 5B, Supplementary Table S21). We found that both mutant isoforms had retained DNA binding at the majority of chromatin binding peaks in the wildtype isoform samples, including known glial differentiation and myelin genes (Figure 5C,D).

The promoter of the *PMP2* gene (which encodes one of the major myelin proteins in Schwann cells) contains a confirmed SOX10 binding site, and SOX10 binding causes *PMP2* transactivation.[43] We performed an electrophoretic mobility shift assay (EMSA) in the SVG fetal glial cells transduced with wildtype and mutant *SOX10* isoforms using a biotin-labeled oligonucleotide corresponding to the *PMP2* promoter region containing the SOX10 binding site (Figure 6A). This analysis revealed that the indel mutant isoforms retained their DNA binding capacity to the SOX10 binding site in the *PMP2* promoter. However, a luciferase reporter assay using a reporter construct with the identical segment of the *PMP2* promoter revealed transactivation by wildtype SOX10 but not by the mutant isoforms (Figure 6B, Supplementary Table S22).

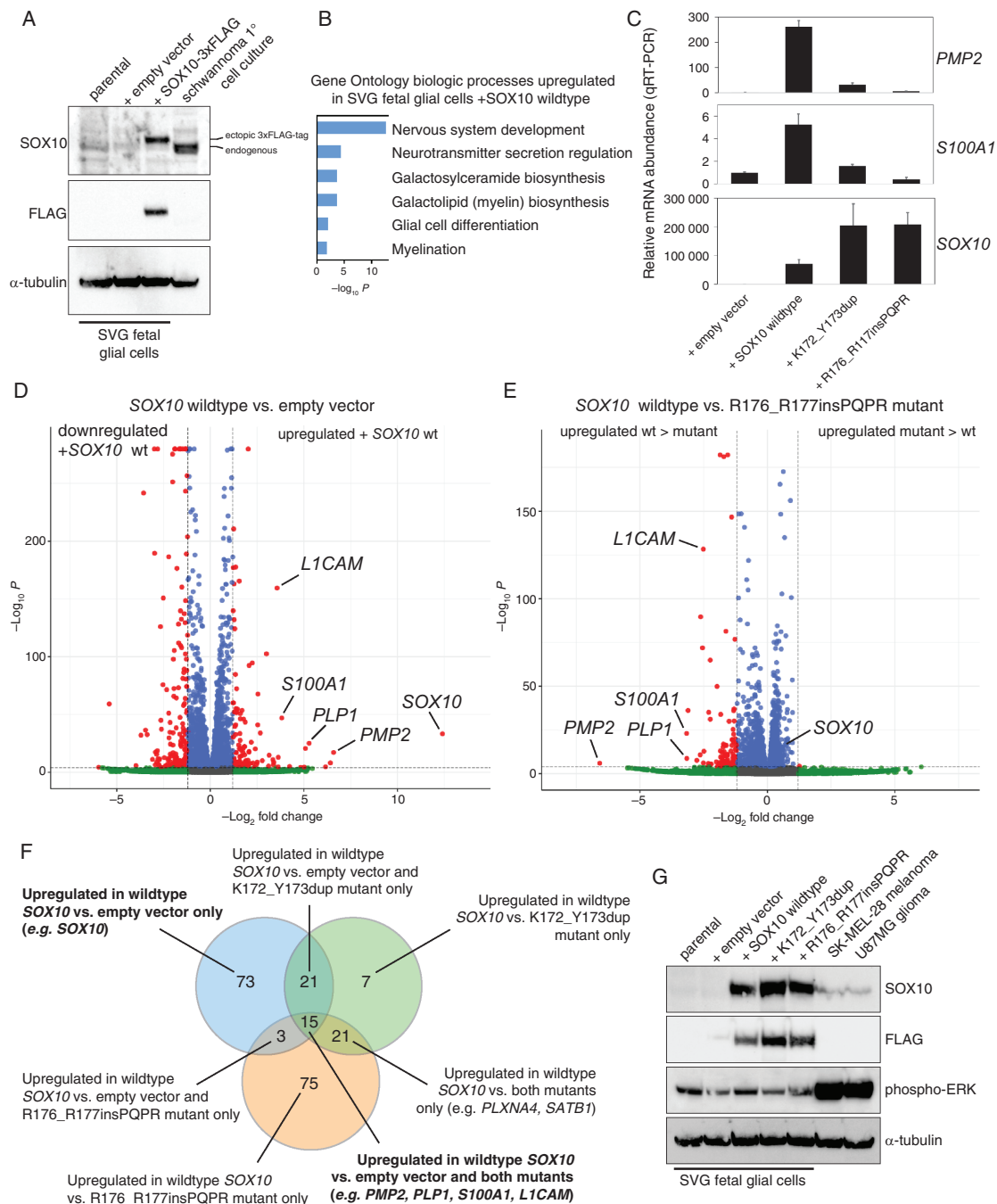In keeping with the observed transactivation of gene programs involved in maturation and terminal

Figure 4. ***SOX10* indel mutations impair transcriptional activation of Schwann cell differentiation and myelination genes.**
(A) Western blots of protein lysates extracted from SVG cells stably transduced with empty vector or FLAG-tagged wildtype *SOX10*, alongside lysate from a primary human schwannoma cell culture for comparison. (B) Gene Ontology analysis showing representative biologic processes that are enriched for genes whose expression is significantly higher in SVG cells transduced with wildtype *SOX10* compared to empty vector. (C) Quantitative reverse transcription-PCR analysis of RNA extracted from SVG cells stably transduced with wildtype and mutant *SOX10* isoforms. Relative gene expression of the indicated targets normalized to *GAPDH* expression is shown, with the mean of 3 replicates per experimental sample plotted with errors bars showing standard deviation. Source data in Supplementary Table S20. (D,E) Volcano plots of whole transcriptome RNA-sequencing gene expression data from SVG fetal glial cells following stable transduction with empty vector, *SOX10* wildtype, or *SOX10* R176_R177insPQPR mutant isoforms. Differentially expressed transcripts with *P*-values of < 1 × 10^{-5} and log2 fold change > 1.2 derived from three sequencing replicates per experimental sample are highlighted in red. See Supplementary Figure S5 for Volcano plot of *SOX10* K172_Y173dup mutant isoform. (F) Venn diagram of RNA-sequencing gene expression data from SVG fetal glial cells following stable transduction with empty vector, *SOX10* wildtype, K172_Y173dup, or R176_R177insPQPR mutant isoforms showing intersection of differentially expressed transcripts. See Supplementary Table S19 for full gene lists. (D) Western blots of protein lysates extracted from SVG cells stably transduced with FLAG-tagged wildtype and mutant *SOX10* isoforms, alongside lysates from parental unmodified SK-MEL-28 melanoma cells and U87MG glioma cells which both have robust MAP kinase signaling pathway activity for comparison.
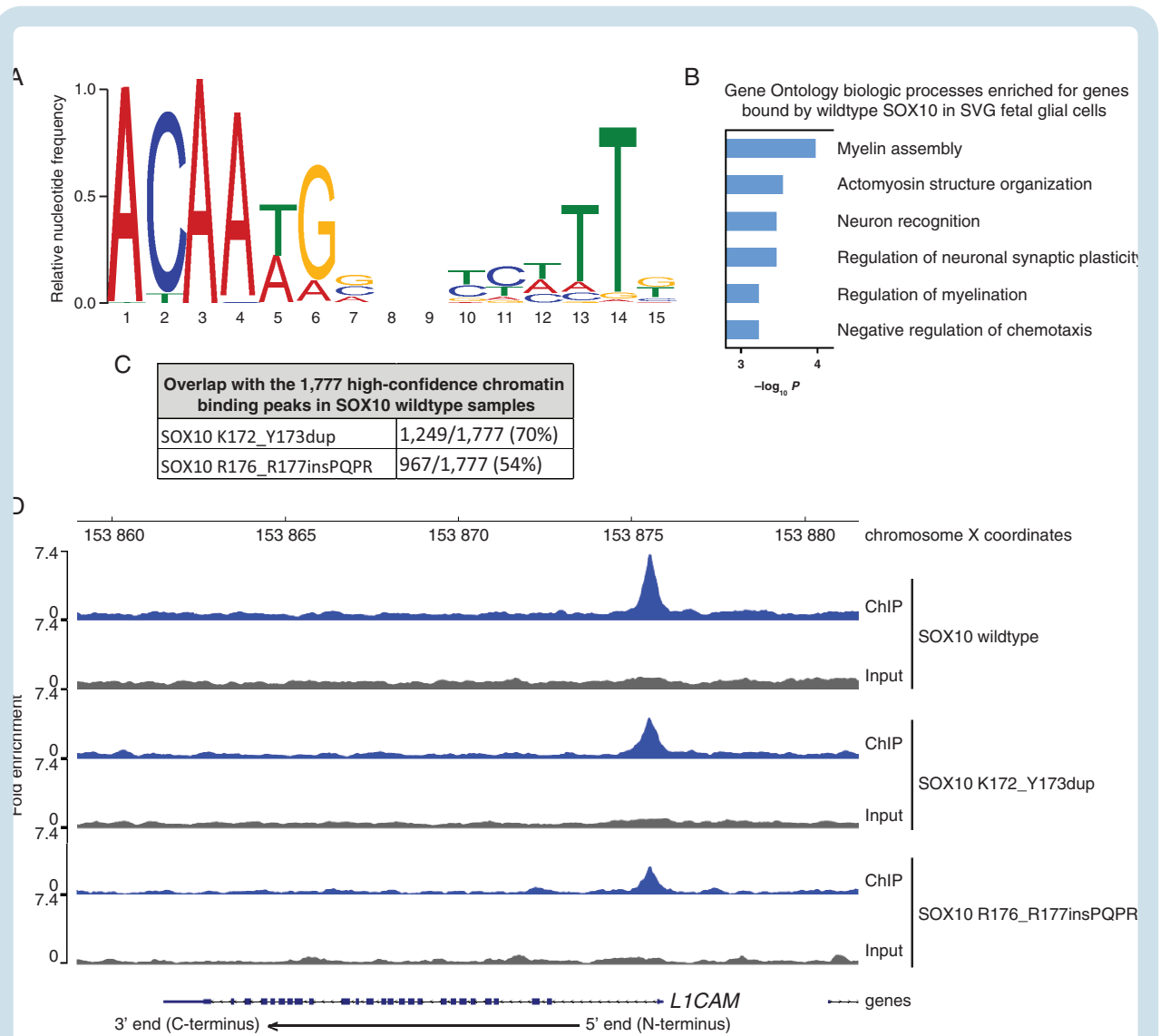
Figure 5. *SOX10* **indel mutant isoforms have retained DNA binding capacity at Schwann cell differentiation and myeli-nation genes.** (A) DNA sequence motif analysis of the 1,777 high-confidence chromatin binding peaks in SVG cells transduced with wildtype *SOX10* revealed the known SOX10 binding motif ACAAAG.[50] (B) Gene Ontology analysis showing representative biologic processes enriched in genes with chromatin binding peaks in the *SOX10* wildtype samples. (C) Overlap of high-confidence chromatin binding peaks between the *SOX10* wildtype samples and the two mutant isoforms. (D) SOX10 chromatin binding peak in the promoter region of the *L1CAM* gene from genome-wide ChIP-sequencing for *SOX10* wildtype and two mutant isoforms. For each pair, the top alignment shows the immunoprecipitation sequencing whereas the bottom shows the input DNA.

differentiation of Schwann cells, expression of wildtype SOX10 was selected against over time in the SVG fetal glial cells (Figure 6C). In contrast, the mutant isoforms continued to be robustly expressed over time under the identical growth conditions, indicating that they did not promote terminal differentiation or halt proliferation (Figure 6C). Based on these findings, we conclude that *SOX10* indel mutations are likely to drive schwannoma development through occupation of SOX10 binding sites but impaired transactivation of Schwann cell differentiation and myelination gene programs, resulting in a persistent immature progenitor-like cell state (Figure 6D).

Discussion

Here we have identified a new recurrent genetic event, *SOX10* indel mutations, occurring in 29% of sporadic schwannomas that is mutually exclusive with all other known nerve sheath molecular drivers. These *SOX10* mutations were enriched in schwannomas arising from non-vestibular cranial nerves, occurred from adolescence through adulthood, and several recurred locally. Intriguingly, we found that *SOX10* indel mutations were absent in vestibular nerve schwannomas, the vast majority
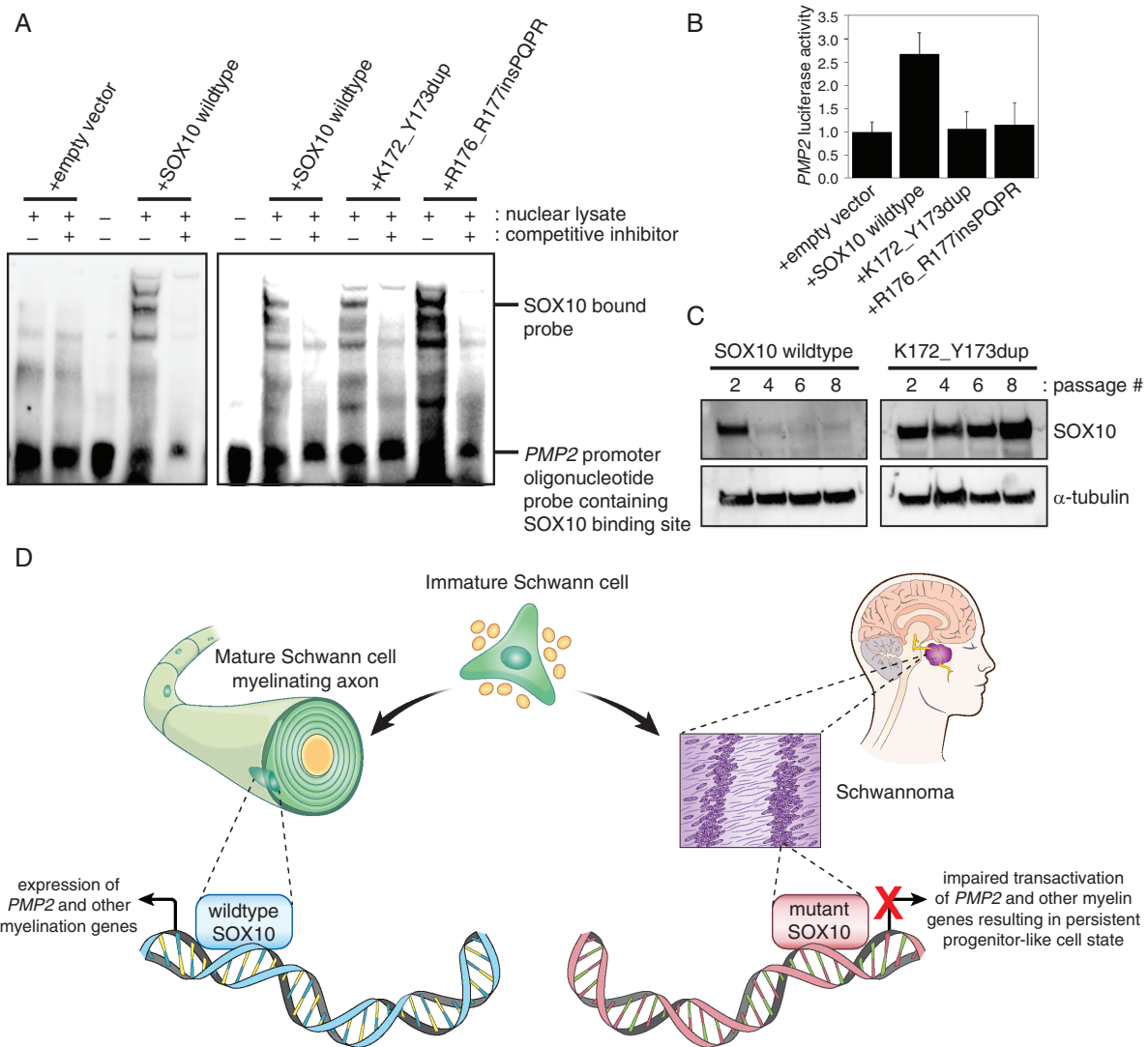
Figure 6. *SOX10* **indel mutations have retained DNA binding capacity but impaired transactivation at the Peripheral Myelin Protein 2 (*PMP2*) gene promoter.** (A) Electrophoretic mobility shift assay (EMSA) of nuclear lysates from SVG cells stably transduced with empty vector, wildtype *SOX10*, or two tumor-derived *SOX10* mutant isoforms using a biotinylated oligonucleotide probe corresponding to a segment of the *PMP2* gene promoter containing a known SOX10 binding site. Binding reactions of the oligonucleotide probe with and without nuclear lysate and unlabeled oligonucleotide competitive inhibitor were resolved on a DNA retarding gel, and SOX10 bound DNA complexes were visualized by chemiluminescence using HRP-conjugated streptavidin. (B) Luciferase reporter assay of a *PMP2* promoter reporter construct containing a known SOX10 binding site transfected into SVG cells stably transduced with empty vector, wildtype *SOX10*, or two *SOX10* indel mutants. Plots show the mean of 3 replicates per experimental sample with errors bars showing standard deviation. Source data in Supplementary Table S22. (C) Western blots of protein lysates extracted from SVG cells stably transduced with SOX10 wildtype and K172_Y173dup mutant isoforms collected over time after the indicated number of serial passages. (D) Model of the role of wildtype *SOX10* in Schwann cell differentiation and mutant *SOX10* in driving schwannoma formation via impaired transcriptional activation of myelination and differentiation gene programs.

of which had *NF2* mutations/deletions. This indicates a propensity for different mechanisms of Schwann cell tumorigenesis depending on anatomic location, perhaps indicating divergent subtypes of specialized Schwann cells that myelinate the vestibular nerve versus other cranial nerves. Furthermore, we identified subtly different epigenetic profiles of *SOX10*-mutant versus *NF2*-mutant schwannomas, which further suggests either a divergent cell of origin or a differential developmental cell state of these two molecularly distinct schwannoma subtypes.

Whereas nerve sheath tumors were primarily thought to arise from genetic aberrations causing hyperactivation of the RAS signaling pathway, our studies have revealed a unique group of schwannomas lacking hyperactivation of RAS signaling and instead driven by blocked differentiation resulting from mutations in the transcription factor responsible for Schwann cell fate determination. Our functional investigation demonstrated that the *SOX10* indel mutant isoforms retain DNA binding capacity but have impaired transactivation of *PMP2* and other

myelination genes, thereby suggesting *SOX10*-mutant schwannomas develop due to impaired differentiation of immature Schwann cells. We are unaware of any other solid tumor type whose central genetic driver is recurrent mutations in a transcription factor responsible for controlling cell fate and differentiation like the *SOX10* indel mutations we have identified in nearly one-third of sporadic schwannomas.

We speculate that the *SOX10* indel mutations we have identified may potentially have been overlooked in prior genomic investigations of schwannomas due to the bioinformatic challenges associated with insertion/deletion detection of this size (mostly 6 to 69 base pairs in length), as sequencing analysis pipelines often focus on single nucleotide variants or short indels less than 3 base pairs in length. As such, our study suggests the potential of other as-yet undiscovered oncogenes and tumor suppressor genes harboring recurrent indel mutations that may have been overlooked to date in the many tumor types wherein no recurrent driver event has yet been detected (eg childhood ependymomas of the posterior fossa, choroid plexus tumors, and many neuroblastomas and medulloblastomas to name just a few). Thus, we advocate to the cancer genomics community for careful evaluation of larger (>3 bp) insertion/deletion mutations and highlight the potential for new discoveries from further analysis of prior cancer genome sequencing datasets.

Given that *SOX10* indel mutations in most schwannomas are present in the heterozygous state with an intact wildtype *SOX10* allele, we postulate that *SOX10* indel mutations may have a dominant tumorigenic effect. As such, suppression of the mutant *SOX10* allele using antisense oligonucleotide technology or other approach may represent a potential therapeutic approach for the treatment of recurrent or unresectable *SOX10*-mutant schwannomas that we aim to explore in future studies.

Supplementary material

Supplementary material is available online at *Neuro-Oncology* (http://neuro-oncology.oxfordjournals.org/).

Keywords

myelination | *PMP2* | Schwann cell | schwannoma | *SOX10*

Authorship statement

All authors made substantial contributions to the conception or design of the study; the acquisition, analysis, or interpretation of data; or drafting or revising the manuscript. All authors approved the manuscript. All authors agree to be personally accountable for individual contributions and to ensure that questions related to the accuracy or integrity of any part of the work are appropriately investigated, resolved, and the resolution documented in the literature. EAW, AR, LJ, JSS, JFC, and DAS designed the study and analyses. Experiments were performed by EAW, AR, NOS, AKS, CH, JW, JB, and DAS. Data analysis was performed by EAW, AR, RG, NOS, AKS, CH, SK, JBY, JW, CGL, MP, JVZ, WPD, ATR, NG, KJW, TAJ, DAM, RSPH, MCH, DCP, GMF, TJ, JSR, LJ, JSS, JFC, and DAS. PEL, TM, AP, AWB, KS, RM, PM, HL, and WHY provided tumor specimens. The study was supervised by EC, SMC, MSB, LJ, JSS, JFC, and DAS. The manuscript and figures were prepared by EAW, AR, RG, and DAS with input from all authors.

Conflict of interest statement

E.A.W., D.A.M., R.S.P.H., M.C.H., D.C.P., G.M.F., T.J., and J.S.R. are employees/consultants of Foundation Medicine, Inc., a wholly owned subsidiary of Roche Holdings, Inc. and Roche Finance Ltd, and these employees have equity interest in an affiliate of these Roche entities. S.M.C., M.S.B., and J.F.C. are editorial board members of *Neuro-Oncology* but were not involved in the handling and decision making for this manuscript. The remaining authors declare no competing interests.

Data Availability

Raw and processed DNA methylation data from the schwannoma cohort has been deposited at the NCBI Gene

Expression Omnibus (GEO) under accession number GSE197094. Digitally scanned image files of representative H&E and immunostained sections from *SOX10* mutant schwannomas are available at the following link: https://figshare.com/projects/Schwannomas_with_SOX10_indel_mutation/172743. Annotated DNA sequencing data from the schwannoma cohort are provided in the supplementary data tables. Raw sequencing data files are available from the authors upon request. Raw and processed RNA-seq and ChIP-seq data from the SVG cells + *SOX10* wildtype and mutant isoforms has been deposited in GEO under accession numbers GSE218097 and GSE234394. All other remaining data are available within the article and supplementary data files, or available from the authors upon request.

Affiliations

Department of Pathology, University of California, San Francisco, San Francisco, California, USA (E.A.W., A.R., R.G., J.W., J.B., C.H.G.L., E.C., M.P., P.E.L., T.M., A.P., A.B., J.V.Z., W.P.D., D.A.S.); Department of Neurological Surgery, University of California, San Francisco, San Francisco, California, USA (N.O.S., A.K.S., C.H., A.P., N.G., S.M.C., M.S.B., L.J., J.F.C.); Department of Physics and Carl R. Woese Institute for Genomic Biology, University of Illinois at Urbana-Champaign, Urbana, Illinois, USA (S.K., J.B.Y., J.S.S.); Departments of Neurology and Pediatrics, University of California, San Francisco, San Francisco, California, USA (A.T.R.); Vista Pathology Laboratory, Medford, Oregon, USA (K.B.); Department of Pathology, Moffitt Cancer Center, Tampa, Florida, USA (R.M.); Department of Pathology, Tampa General Hospital, Tampa, Florida, USA (P.M.); Department of Pathology, University of California, Davis, Sacramento, California, USA (H.L.); Department of Pathology and Laboratory Medicine, University of California, Irvine, Irvine, California, USA (W.H.Y.); Departments of Physiology and Medicine, Lewis Katz School of Medicine, Temple University, Philadelphia, Pennsylvania, USA (K.J.W.); Department of Neurosurgery, Division of Neuro-Oncology, Faculty of Medicine and Carl Gustav Carus University Hospital, Dresden, Germany (T.A.J.); Foundation Medicine, Inc., Cambridge, Massachusetts, USA (D.A.M., R.S.P.H., M.C.H., D.C.P., G.M.F., T.J., J.S.R.); Department of Pathology, State University of New York Upstate Medical University, Syracuse, New York, USA (J.S.R.).

References

1. Helbing DL, Schulz A, Morrison H. Pathomechanisms in schwannoma development and progression. *Oncogene*. 2020;39(32):5421–5429.
2. Trofatter JA, MacCollin MM, Rutter JL, et al. A novel moesin-, ezrin-, radixin-like gene is a candidate for the neurofibromatosis 2 tumor suppressor. *Cell*. 1993;72(5):791–800.
3. Hulsebos TJ, Plomp AS, Wolterman RA, et al. Germline mutation of INI1/SMARCB1 in familial schwannomatosis. *Am J Hum Genet*. 2007;80(4):805–810.
4. Sestini R, Bacci C, Provenzano A, Genuardi M, Papi L. Evidence of a four-hit mechanism involving SMARCB1 and NF2 in schwannomatosis-associated schwannomas. *Hum Mutat*. 2008;29(2):227–231.
5. Piotrowski A, Xie J, Liu YF, et al. Germline loss-of-function mutations in LZTR1 predispose to an inherited disorder of multiple schwannomas. *Nat Genet*. 2014;46(2):182–187.
6. Mansouri S, Suppiah S, Mamatjan Y, et al. Epigenomic, genomic, and transcriptomic landscape of schwannomatosis. *Acta Neuropathol*. 2021;141(1):101–116.
7. Twist EC, Ruttledge MH, Rousseau M, et al. The neurofibromatosis type 2 gene is inactivated in schwannomas. *Hum Mol Genet*. 1994;3(1):147–151.
8. Irving RM, Moffat DA, Hardy DG, et al. Somatic NF2 gene mutations in familial and non-familial vestibular schwannoma. *Hum Mol Genet*. 1994;3(2):347–350.
9. Lekanne Deprez RH, Bianchi AB, Groen NA, et al. Frequent NF2 gene transcript mutations in sporadic meningiomas and vestibular schwannomas. *Am J Hum Genet*. 1994;54(6):1022–1029.
10. Sainz J, Huynh DP, Figueroa K, et al. Mutations of the neurofibromatosis type 2 gene and lack of the gene product in vestibular schwannomas. *Hum Mol Genet*. 1994;3(6):885–891.
11. Agnihotri S, Jalali S, Wilson MR, et al. The genomic landscape of schwannoma. *Nat Genet*. 2016;48(11):1339–1348.
12. Håvik AL, Bruland O, Myrseth E, et al. Genetic landscape of sporadic vestibular schwannoma. *J Neurosurg*. 2018;128(3):911–922.
13. Gao X, Zhang L, Jia Q, et al. Whole genome sequencing identifies key genes in spinal schwannoma. *Front Genet*. 2020;11:507816.
14. Britsch S, Goerich DE, Riethmacher D, et al. The transcription factor Sox10 is a key regulator of peripheral glial development. *Genes Dev*. 2001;15(1):66–78.
15. Finzsch M, Schreiner S, Kichko T, et al. Sox10 is required for Schwann cell identity and progression beyond the immature Schwann cell stage. *J Cell Biol*. 2010;189(4):701–712.
16. Fujiwara S, Hoshikawa S, Ueno T, et al. SOX10 transactivates S100B to suppress Schwann cell proliferation and to promote myelination. *PLoS One*. 2014;9(12):e115400.
17. Pingault V, Bondurand N, Kuhlbrodt K, et al. SOX10 mutations in patients with Waardenburg-Hirschsprung disease. *Nat Genet*. 1998;18(2):171–173.
18. Kuhlbrodt K, Schmidt C, Sock E, et al. Functional analysis of Sox10 mutations found in human Waardenburg-Hirschsprung patients. *J Biol Chem*. 1998;273(36):23033–23038.
19. Bondurand N, Dastot-Le Moal F, Stanchina L, et al. Deletions at the SOX10 gene locus cause Waardenburg syndrome types 2 and 4. *Am J Hum Genet*. 2007;81(6):1169–1185.
20. Kline CN, Joseph NM, Grenert JP, et al. Targeted next-generation sequencing of pediatric neuro-oncology patients improves diagnosis, identifies pathogenic germline mutations, and directs targeted therapy. *Neuro Oncol*. 2017;19(5):699–709.
21. Goode B, Mondal G, Hyun M, et al. A recurrent kinase domain mutation in PRKCA defines chordoid glioma of the third ventricle. *Nat Commun*. 2018;9(1):810.
22. Talevich E, Shain AH, Botton T, Bastian BC. CNVkit: genome-wide copy number detection and visualization from targeted DNA sequencing. *PLoS Comput Biol*. 2016;12(4):e1004873.
23. Frampton GM, Fichtenholtz A, Otto GA, et al. Development and validation of a clinical cancer genomic profiling test based on massively parallel DNA sequencing. *Nat Biotechnol*. 2013;31(11):1023–1031.
24. Aryee MJ, Jaffe AE, Corrada-Bravo H, et al. Minfi: a flexible and comprehensive Bioconductor package for the analysis of Infinium DNA methylation microarrays. *Bioinformatics*. 2014;30(10):1363–1369.
25. Fortin JP, Labbe A, Lemire M, et al. Functional normalization of 450k methylation array data improves replication in large cancer studies. *Genome Biol*. 2014;15(11):503.

26. Triche TJ, Jr, Weisenberger DJ, Van Den Berg D, Laird PW, Siegmund KD. Low-level processing of Illumina Infinium DNA methylation BeadArrays. *Nucleic Acids Res.* 2013;41(7):e90.

27. Capper D, Jones DTW, Sill M, et al. DNA methylation-based classification of central nervous system tumours. *Nature.* 2018;555(7697):469–474.

28. Koelsche C, Schrimpf D, Stichel D, et al. Sarcoma classification by DNA methylation profiling. *Nat Commun.* 2021;12(1):498.

29. Gu Z, Eils R, Schlesner M. Complex heatmaps reveal patterns and correlations in multidimensional genomic data. *Bioinformatics.* 2016;32(18):2847–2849.

30. Peters TJ, Buckley MJ, Statham AL, et al. De novo identification of differentially methylated regions in the human genome. *Epigenetics Chromatin.* 2015;8:6.

31. Kim D, Langmead B, Salzberg SL. HISAT: a fast spliced aligner with low memory requirements. *Nat Methods.* 2015;12(4):357–360.

32. Love MI, Huber W, Anders S. Moderated estimation of fold change and dispersion for RNA-seq data with DESeq2. *Genome Biol.* 2014;15(12):550.

33. Blighe K, Rana S, Lewis M. EnhancedVolcano: publication-ready volcano plots with enhanced colouring and labeling; 2018. https://github.com/kevinblighe/EnhancedVolcano

34. Langmead B, Salzberg SL. Fast gapped-read alignment with Bowtie 2. *Nat Methods.* 2012;9(4):357–359.

35. Li H, Handsaker B, Wysoker A, et al; 1000 Genome Project Data Processing Subgroup. The Sequence Alignment/Map format and SAMtools. *Bioinformatics.* 2009;25(16):2078–2079.

36. Ramirez F, Ryan DP, Gruning B, et al. deepTools2: a next generation web server for deep-sequencing data analysis. *Nucleic Acids Res.* 2016;44(W1):W160–W165.

37. Zhang Y, Liu T, Meyer CA, et al. Model-based analysis of ChIP-Seq (MACS). *Genome Biol.* 2008;9(9):R137.

38. Li Q, Brown JB, Huang H, Bickel PJ. Measuring reproducibility of high-throughput experiments. *Ann. Appl. Stat.* 2011;5(3):1752–1779.

39. McLean CY, Bristor D, Hiller M, et al. GREAT improves functional interpretation of cis-regulatory regions. *Nat Biotechnol.* 2010;28(5):495–501.

40. Ashburner M, Ball CA, Blake JA, et al. Gene ontology: tool for the unification of biology. The Gene Ontology Consortium. *Nat Genet.* 2000;25(1):25–29.

41. Bailey TL. STREME: accurate and versatile sequence motif discovery. *Bioinformatics.* 2021;37(18):2834–2840.

42. Bailey TL, Johnson J, Grant CE, Noble WS. The MEME suite. *Nucleic Acids Res.* 2015;43(W1):W39–W49.

43. Graf SA, Heppt MV, Wessely A, et al. The myelin protein PMP2 is regulated by SOX10 and drives melanoma cell invasion. *Pigment Cell Melanoma Res.* 2019;32(3):424–434.

44. Vasudevan HN, Lucas CG, Villanueva-Meyer JE, Theodosopoulos PV, Raleigh DR. Genetic events and signaling mechanisms underlying Schwann cell fate in development and cancer. *Neurosurgery.* 2021;88(2):234–245.

45. Ronellenfitsch MW, Harter PN, Kirchner M, et al. Targetable ERBB2 mutations identified in neurofibroma/schwannoma hybrid nerve sheath tumors. *J Clin Invest.* 2020;130(5):2488–2495.

46. Kirschner LS, Carney JA, Pack SD, et al. Mutations of the gene encoding the protein kinase A type I-alpha regulatory subunit in patients with the Carney complex. *Nat Genet.* 2000;26(1):89–92.

47. Machon O, Masek J, Machonova O, Krauss S, Kozmik Z. Meis2 is essential for cranial and cardiac neural crest development. *BMC Dev Biol.* 2015;15:40.

48. Bigenzahn JW, Collu GM, Kartnig F, et al. LZTR1 is a regulator of RAS ubiquitination and signaling. *Science.* 2018;362(6419):1171–1177.

49. Steklov M, Pandolfi S, Baietti MF, et al. Mutations in LZTR1 drive human disease by dysregulating RAS ubiquitination. *Science.* 2018;362(6419):1177–1182.

50. Srinivasan R, Sun G, Keles S, et al. Genome-wide analysis of EGR2/SOX10 binding in myelinating peripheral nerve. *Nucleic Acids Res.* 2012;40(14):6449–6460.